The capsid of small papova viruses contains 72 pentameric capsomeres: direct evidence from cryo-electron-microscopy of simian virus 40

Timothy S. Baker,* Jacqueline Drak,‡ and Minou Bina‡
*Department of Biological Sciences, and ‡Department of Chemistry, Purdue University, West Lafayette, Indiana 47907

ABSTRACT The three-dimensional structure of the simian virus 40 capsid is remarkably similar to the structure of the polyoma empty capsid. This similarity is apparent despite striking differences in the methods used to determine the two structures: image analysis of electron micrographs of frozen-hydrated samples (SV40 virions) and an unconventional x-ray crystallographic analysis (polyoma empty capsids). Both methods have clearly resolved the 72 prominent capsomere units which comprise the T = 7d icosahedral capsid surface lattice. The 12 pentavalent and 60 hexavalent capsomeres consist of pentameric substructures. A pentameric morphology for hexavalent capsomeres clearly shows that the conserved bonding specificity expected from the quasi-equivalence theory is not present in either SV40 or polyoma capsids. Determination of the SV40 structure from cryo-electron microscopy supports the correctness of the polyoma structure solved crystallographically and establishes a strong complementarity of the two techniques. Similarity between the SV40 virion and the empty polyoma capsid indicates that the capsid is not detectably altered by the loss of the nucleohistone core. The unexpected pentameric substructure of the hexavalent capsomeres and the arrangement of the 72 pentamers in the SV40 and polyoma capsid lattices may be characteristic features of all members of the papova virus family, including the papilloma viruses such as human wart and rabbit papilloma.

INTRODUCTION

Interest in the structure of papova viruses has been quite high ever since the first electron micrographs of rabbit papilloma were published (Sharp et al., 1942). Papova is an acronym used to describe **pa**pilloma, **po**lyoma, and **va**cuolating agent (SV40) type viruses (Melnick, 1962). On the basis of their morphological characteristics and their biochemical composition, the papova viruses have been classified into two genera. The *A* genus comprises the papilloma viruses. These have been identified in many animal species, but the human and bovine viruses have been among those most extensively examined (Tooze, 1981). The *B* genus includes SV40, polyoma, and the human JC- and BK-type viruses (Tooze, 1981). Even though the viruses of the B-genus exhibit similar physical and biological properties, SV40 and polyoma have been favored for extensive biochemical, genetic, and structural studies, in part, because these viruses are readily propagated in the appropriate cell lines cultured in the laboratory. In addition, both viruses have served as model systems for studying molecular aspects of viral assembly, genetic regulation, and the mechanisms involved in transformation of mammalian cells.

Table 1 provides a summary of the components present in the mature virion particles isolated from cells infected with SV40 or polyoma. Each virion contains a single double-stranded DNA molecule which is circular and covalently-closed. The current evidence indicate that the assembly of SV40 and polyoma virions follows a stepwise process (reviewed by Bina, 1986). The viral DNA is initially condensed by the cellular core histones into repeating units (nucleosomes) formed from wrapping 146–200 base pairs of DNA around histone octamers (two molecules each of H2A, H2B, H3, and H4). The resulting nucleohistone complex is known as a minichromosome (Griffith, 1975). The virion proteins (VP1, VP2, and VP3) are subsequently added to the minichromosome to form the virion particles isolated from infected cells (Blasquez et al., 1983). VP1 accounts for nearly 80% of the total virion protein (reviewed by Baker and Rayment, 1987), Table 1. Empty capsids isolated from infected cells are not virion precursors but result when virions dissociate during isolation procedures (Garber et al., 1979; Fernandez-Munoz et al., 1979; Baumgartner et al., 1979; Yuen et al., 1985).

Studies conducted on the structure of papova viruses have historically been marked by controversy and surprise. A major debate arose when attempts were made to determine the number and arrangement of the morphological units forming the capsid (Mattern, 1962; Mayor and Melnick, 1962). Two conflicting models were proposed: one favoring a capsid consisting of 42 morphological units (Wildy et al., 1960; Melnick, 1962), while the

Address all correspondence to Timothy S. Baker.
Dr. Drak's present address is Department of Chemistry, Yale University, New Haven, Connecticut 06511

0006-3495/89/02/243/11 $2.00

TABLE 1 Comparison of the components and structural features of SV40 and polyoma

	SV40 (776 strain)	Polyoma (A2 strain)
Diameter (nm)	49.4	49.5
Capsid symmetry (T number)	7*d*	7*d*
Virion DNA content		
(% wt/wt) ≃	12.5%	13.8%
1 mol/double stranded circular/covalently closed	5243 bp	5292 bp
M_r	3.24×10^6	3.27×10^6
Virion protein composition		
VP1 ≃ 79% major total protein		
Number of amino acid residues	361	382
M_r	40,168	42,404
Number of copies/virion	360	360
VP2		
M_r	38,351	34,761
Number of amino acid residues	351	318
Number of copies/virion ≃	ND	≃28
VP3		
M_r	26,965	22,866
Number of amino acid residues	233	203
Number of copies/virion	ND	≃24
Core Histones		
M_r		
H3	15,300	15,300
H2A	14,000	14,000
H2B	13,800	13,800
H4	11,300	11,300
Core Histone/DNA (wt/wt)	≃1	≃1
Topoisomerase	+	ND

Abbreviations: bp, base pairs; ND, not determined.
The diameter of SV40 virions was measured from micrographs of frozen-hydrated samples, using polyoma as a standard (Olson and Baker, manuscript submitted for publication). The diameter of polyoma represents the packing distance in crystals (Rayment et al., 1982). The molecular weights of the virion proteins were calculated from sequence data (Tooze, 1981). The number of copies of VP2 and VP3 in polyoma are estimates based on densitometry of stained gels (W. T. Murakami, personal communication).

other favored a capsid constructed from 92 units (Mattern, 1962). Both models were based on interpretation of micrographs of negatively-stained virus particles and the expectation that the capsid structure would conform to the empirical rules derived for predicting the number of morphological units present on the surface of spherical viruses (Horne and Wildy, 1961). A 72-unit structure, which later proved correct, was subsequently proposed by Caspar and Klug (1962) as a more likely alternative to the 42-unit and 92-unit models.

The pioneering work of Caspar and Klug (1962) brought forth a theory to explain why capsid protein subunits in simple spherical viruses self-assemble with icosahedral symmetry. A capsid with strict icosahedral symmetry is expected to consist of $60T$ identical copies of the capsid subunits. The T (triangulation) number defines the lattice symmetry of the icosahedron and should equal the number of subunits in each of the 60 asymmetric units of the icosahedron. Due to symmetry constraints, T only assumes certain values (e.g., 1, 3, 4, 7, 9, 12, 13 . . .). The theory predicts that a capsid with $T = 1$ lattice symmetry consists of 60 identical subunits, all in strictly identical (equivalent) environments whereas a larger or more complex capsid with $T = 7$ symmetry is expected to consist of 420 ($=60 \times 7$) subunits, quasi-equivalently arranged. Since a $T = 7$ lattice consists of 12 pentavalent (five-coordinated) and 60 hexavalent (six-coordinated) positions, a capsid consisting of 72 morphological units (capsomeres) could arise if 420 identical protein subunits cluster as 12 pentamers at the pentavalent positions and 60 hexamers at the hexavalent positions.

Electron microscopy and image analysis of negatively stained samples of SV40 and polyoma virions established that the capsid indeed consists of 72 capsomeres arranged on a right-handed $T = 7$ icosahedral lattice (Klug, 1965; Anderer et al., 1967; Finch, 1974). Similar studies have demonstrated that the capsids of papilloma viruses also consist of 72 capsomeres (Klug and Finch, 1965; Finch and Klug, 1965). Surprisingly, the rabbit papilloma is left handed ($T = 7l$), while the human wart papilloma is right handed ($T = 7d$). A three-dimensional reconstruction of polyoma virus revealed that the sizes of the pentavalent and hexavalent capsomeres are nearly identical (Finch, 1974). To account for this result and maintain a 420-subunit structure, Finch (1974) suggested that the capsid consists of 60 hexamers of the major virion protein (VP1), occupying the 60 hexavalent lattice positions, and 12 pentamers of either VP2, or VP3, or both, occupying the 12 pentavalent lattice positions. This interpretation accommodates the results reported in earlier work concerning the stoichiometry of the three virus-coded proteins (Friedmann and David, 1972).

The unexpected discovery (Rayment et al., 1982) that both the hexavalent and pentavalent capsomeres present in the polyoma empty capsid consist of pentamers of VP1 indicates that the entire capsid is composed of 360 VP1 subunits, in which bonding specificity is not conserved as formulated by Caspar and Klug (1962). Questions were raised (Eisenberg, 1982; Klug, 1983) concerning the results obtained by Rayment et al. (1982) since the structure was solved using a novel crystallographic method in which structure factor phases, derived from computer generated models, were combined with diffraction amplitudes measured from x-ray precession photographs of native capsid crystals.

We have recently solved the structure of the SV40 virion, using cryo-electron microscopy and image analysis

(Baker et al., 1988), at a resolution comparable to the x-ray analysis of polyoma empty capsids (Rayment et al., 1982). Here, we describe the criteria used to determine the SV40 virion structure and compare the capsid structures of SV40 and polyoma. The observed similarities help resolve uncertainties concerning the validity of the procedures used to solve the polyoma structure. The structure of SV40 and polyoma explains and reconciles observations made previously in the analysis of negatively stained polyoma specimens (Finch, 1974).

MATERIALS AND METHODS

Sample preparation and electron microscopy

Mature wt776 virions were isolated as previously described (Bina et al., 1982; Baker et al., 1988). Aqueous samples (3–4 μl) of SV40 virions (≈4 mg/ml in 12.5 mM Tris buffer at pH 7.4) were applied to holey, carbon-coated grids made hydrophilic by glow discharge in an atmosphere of amyl-amine, blotted with filter paper for a few seconds, and rapidly plunged into liquid ethane (Milligan et al., 1984). Grids were transferred under liquid nitrogen to a Gatan cold holder (Gatan, Inc. 780 Commonwealth Drive, Warrendale, PA) which maintained the specimen at ~ −160°C in the electron microscope. The micrographs were recorded on Kodak SO-163 film (Eastman Kodak Company, Rochester, NY) using low-irradiation conditions (≈1,000 e^-/nm^2) on an EM400 electron microscope (Philips Electronic Instruments, Mahwah, NJ) operated at 100 kV at a nominal magnification of X33,000. The actual magnification (X27,000) was determined using polyoma virus as a calibration standard (Olson and Baker, manuscript submitted for publication).

Image analysis and three-dimensional reconstruction

The micrograph selected for computing the three-dimensional reconstructions was recorded with the objective lens underfocused by 1–2 μm (Fig. 1), a level of defocus at which the phase contrast transfer function (CTF) of the microscope remains positive for all spatial frequencies within the 3.8 nm resolution limit of the reconstructions (Erickson and Klug, 1971). Corrections for nonlinearities of the CTF (Lepault and Leonard, 1985) were not made since they did not significantly alter the subsequent reconstructions.

Three separate three-dimensional reconstructions were computed as described before (Baker et al., 1988), using procedures similar to those developed to analyze negatively-stained icosahedral particles (Crowther et al., 1970, *a* and *b*; Crowther, 1971). A region of the selected micrograph (Fig. 1) was digitized at regular intervals (25 μm), corresponding to ≈0.92 nm at the specimen, and displayed using a raster graphics device (model 3400; Lexidata Corp., Billerica, MA). Randomly selected particles were masked from their surroundings with circular boundaries. Each particle image was floated (DeRosier and Moore, 1970) and Fourier transformed and the center of each particle was initially located using a cross-correlation procedure (Olson and Baker, manuscript submitted for publication). The original common lines method (Crowther, 1971) was modified to refine the view orientation (θ, ϕ, ω) and center of each particle to a unique solution in a few cycles of an iterative procedure (Fuller, 1987; Baker et al., 1988). The mean phase residual computed from the common lines procedure was used to check the extent to which the particle transforms are consistent with their having arisen from a structure with icosahedral symmetry. The particle images used in the reconstructions all showed some correlation with icosahedral symmetry to spatial frequencies of 3 to 4 nm (Fig. 4).

To compute the three-dimentional structure of SV40, one particle image was chosen as reference and the remaining set of images were scaled to the same magnification and contrast. The scaled data were combined, taking into account the relative orientations of the particles, to produce a three-dimensional Fourier transform. Electron density maps were computed by inverse Fourier-Bessel transformation of the three-dimensional transform after constraining it to obey D_5 symmetry (Crowther, 1971). The maps were displayed with a right-handed surface lattice ($T = 7d$), consistent with the earlier hand determination of SV40 (Anderer et al., 1967).

RESULTS AND DISCUSSION

Electron microscopy and image analysis

The structure of SV40 virions was examined using the cryo-electron microscopy technique (Adrian et al., 1984; Milligan et al., 1984) since this method preserves the native morphology of biological macromolecules and produces images in which contrast is related to genuine differences in mass density. The cryo-method offers significant advantages over the traditional preparative procedures such as negative-staining, metal shadowing or embedding and thin-sectioning, since it does not require dehydration of the specimen or the addition of stains or heavy metal atoms to enhance contrast.

Fig. 1 shows a field of frozen-hydrated SV40 virions, recorded using low-irradiation conditions to minimize radiation induced damage to the sample (Williams and Fisher, 1970; Baker and Amos, 1978). This micrograph was selected from over one-hundred recorded since it showed minimal drift or vibration resulting from instabilities of the cold stage, minimal residual image astigmatism, and an optimal level of underfocus which maximized positive phase contrast in the 3 to 4 nm resolution range (Baker et al., 1988). Furthermore, the selected micrograph (Fig. 1) was recorded from a region of the specimen containing a concentrated, mono-disperse distribution of virus particles in a uniform layer of vitreous ice approximately as thick as the SV40 particles (50 nm). Most of the individual SV40 virion particles have nearly circular image profiles indicating that particle flattening did not occur and that the spherical particle shape is well preserved by the preparative technique (Fig. 1).

Close inspection of the particle images in Fig. 1 reveals that the virions are randomly oriented in the thin specimen. The projected view of an individual virus particle arises from the superposition of density in the entire particle since the depth of field in the electron microscope is larger than the thickness of the frozen-hydrated speci-

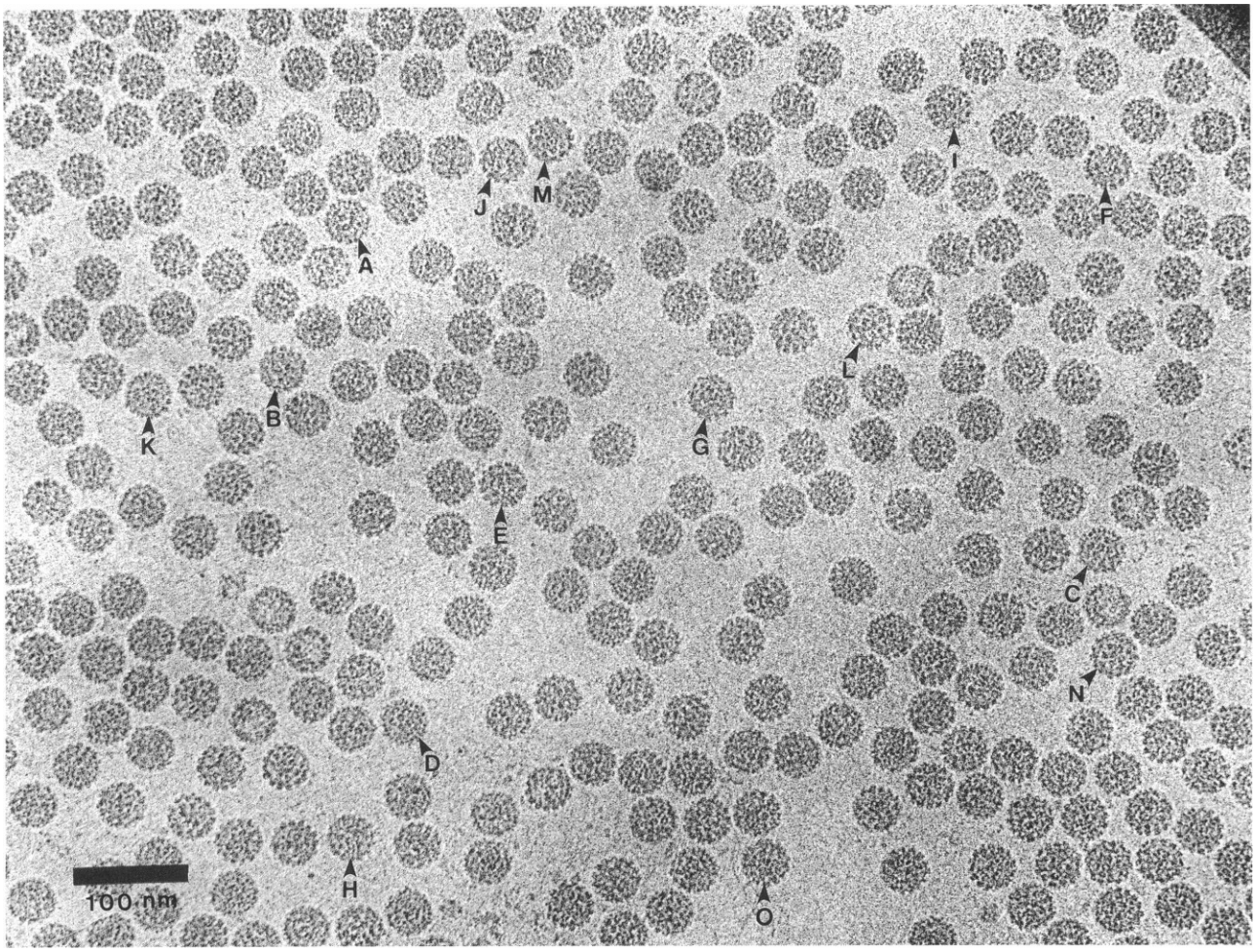

FIGURE 1 High magnification view of a frozen-hydrated SV40 sample. Individual virus particles are suspended over a hole in the carbon substrate within a thin layer of vitreous ice about the same thickness (≈50 nm) as the particle diameter. Particle contrast is significantly reduced in regions where the ice is too thick (>100 nm; not shown). Despite the high level of noise in this slightly defocused image (1–2 μm), the capsomere units and random orientation of the particles are clearly evident (Low contrast in the original micrograph is photographically enhanced here to better display these characteristic features). Most particles display circular outlines, indicating good preservation of the spherical shape and symmetry. The 15 particles, labeled A–O, were randomly selected and analyzed to determine the relative viewing directions and to combine the images for computing the three-dimensional reconstruction (displayed in Fig. 6).

men. A characteristic feature of the structure of papova viruses is that the superposition of the images of the 72 capsomeres produces a distinct pattern for each particle depending on its orientation. This feature is a critical factor in objectively identifying a suitable number of different views for determining the three-dimensional structure of the virus using image analysis procedures (Crowther et al., 1970, *a*, *b*; Crowther, 1971).

In a typical field of unstained, frozen-hydrated SV40 virions, it is relatively easy to identify particles oriented with an icosahedral three-fold axis in the direction of view (e.g., particles *A* and *D* in Fig. 1). Particles viewed near a five-fold axis of symmetry are occasionally seen (*N*, Fig. 1), but images of two-fold views are more difficult to detect. The ease with which three- and five-fold views can be recognized is mainly a consequence of the strikingly characteristic features at low resolution (3 to 4 nm) arising from the superposition of images of the capsomeres on opposite sides of the virus shell. Projection of structural details along the two-fold direction gives rise to features which are too fine to detect above the noise level in unaveraged images.

The quality of individual images of particles in the selected micrograph viewed close to three- and five-fold symmetry axes (Fig. 1) was assessed quantitatively using rotational power spectrum analysis (Crowther and Amos, 1971; Baker et al., 1985). To establish the presence of rotational symmetry for objects the size of SV40, the

image view must be within one or two degrees of a symmetry axis. Fig. 2 shows rotational power spectra computed for the two particle images labeled *A* and *N* in Fig. 1. The distribution of intense peaks provides strong evidence for three-fold (Fig. 2 *A*) and five-fold (Fig. 2 *D*) rotational symmetries in the respective digitized images (Fig. 2, *B* and *E*). The quality of these spectra indicate that the symmetries of both particles were well preserved during the cryo-electron microscopic procedures.

Particle images of *A* and *N* were rotationally filtered to reduce the noise and enhance the symmetry related features. The averaged images were reconstructed using only those Fourier components that are multiples of the expected *n*-fold symmetry (Crowther and Amos, 1971). The filtered images appear striking, but they only provide two-dimensional projected views of the virus (Fig. 2, *C* and *F*). The three distinct pentameric substructures in the center of the three-fold average image (Fig. 2 *C*) give the impression that only one side of the particle is imaged. In fact, in this projected view, the clear pentameric substructure is mainly observed owing to: (*a*) near perfect superposition of the hexavalent capsomeres on the opposite sides of the capsid and (*b*) alignment of the axes of these capsomeres nearly parallel to the icosahedral three-fold axis. When viewed along the particle five-fold axis (Fig. 2 *F*), the superimposed images of the hexavalent capsomeres are not clearly resolved because the capsomere images from opposite sides do not superimpose exactly and because the axes of the capsomeres are tilted away from the five-fold axis.

The presence of pentameric substructure in the hexavalent capsomeres was firmly established when the three-dimensional reconstruction of the virus was computed. We selected additional images of particles not viewed

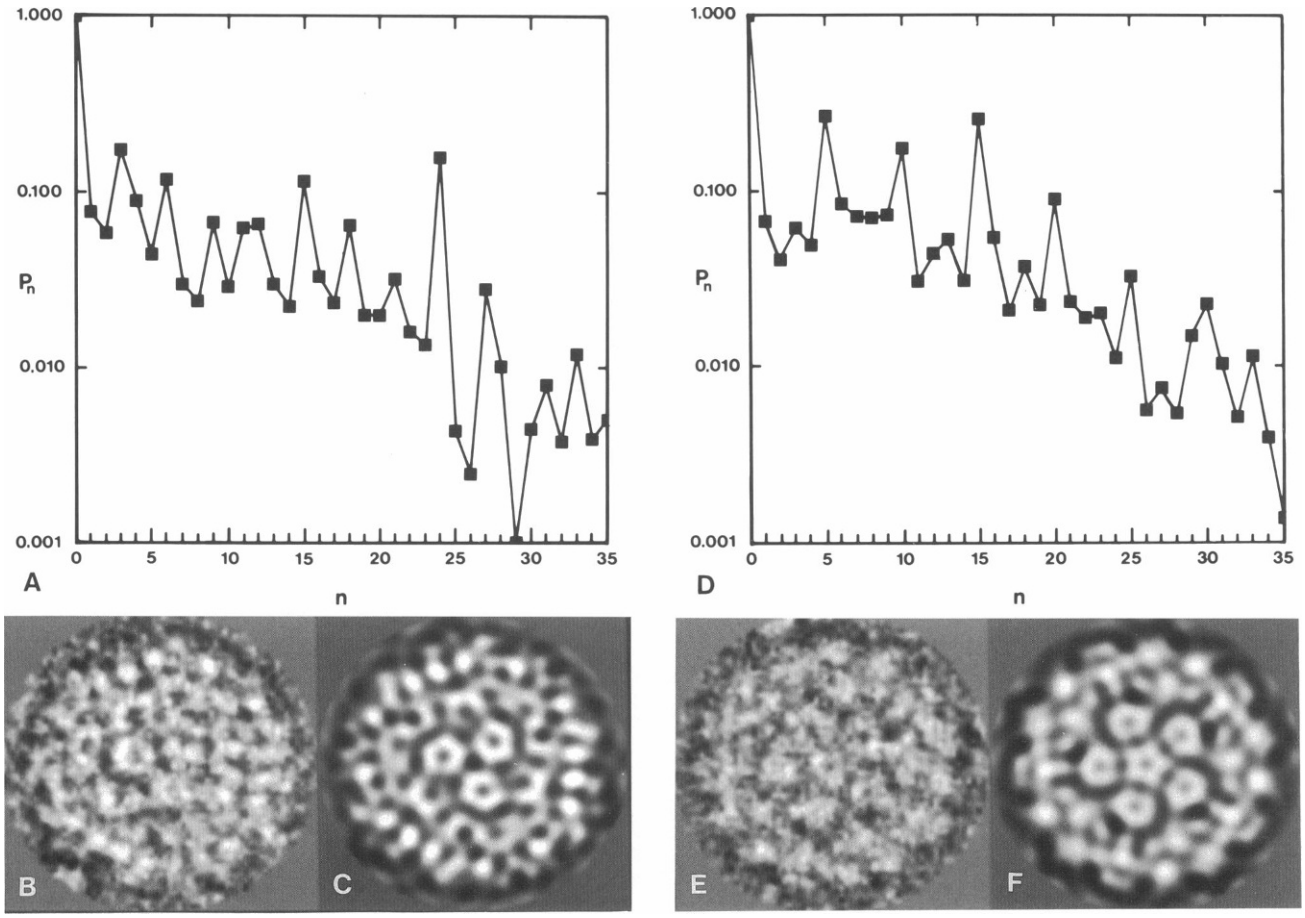

FIGURE 2 Logarithmic plots (A, D) of the rotational power spectra of two SV40 particle images (B, E) reveal dominant 3-fold and 5-fold symmetries. The curves are normalized with $P_o = 1$. For rotational frequencies higher than $n = 35$ the power is <0.001. B and E are highly magnified views (with contrast reversed and enhanced) corresponding to particles labeled D, viewed close to an icosahedral three-fold axis, and N, viewed close to a five-fold axis, of Fig. 1. Rotationally filtered images (C, F), were computed using a Fourier-Bessel synthesis of only those rotational components from B and E which are multiples of three or five. The filtered images show considerable detail not apparent in the noisy, unfiltered images.

along strict icosahedral symmetry axes from the micrograph shown in Fig. 1. We subsequently followed a modification (Fuller, 1987; Baker et al., 1988) of the original common lines method, (Crowther, 1971) in order to refine both the view orientation, (θ, ϕ, ω; Klug and Finch, 1968) and center (origin of symmetry axes) of each particle, and to assess particle quality. The θ, ϕ orientations determined for the final set of selected particle images illustrate that the views used in the reconstruction are fairly uniformly distributed within the asymmetric unit of the icosahedron (Fig. 3). This wide distribution of view orientations and the redundancy generated by the known symmetry of the capsid provide sufficient data to reconstruct the three-dimensional structure of the virus.

The extent to which the expected icosahedral symmetry was obeyed for each particle was assessed quantitatively by computing the mean phase difference between pairs of common lines in the Fourier transform of each digitized virus image (Fig. 4). The common lines are pairs of lines along which, due to the symmetry of the particle, the transform should be the same (Crowther, 1971). Fig. 4 plots the mean phase residuals as a function of resolution for the best (particle L), the worst (particle H) and the average of the images used in the subsequent three-dimensional analysis. Particles with low residuals are those in which icosahedral symmetry is best preserved. In images of unstained, frozen-hydrated particles, the noise level is typically higher than that detected in negatively-stained specimens, especially at the high spatial frequen-

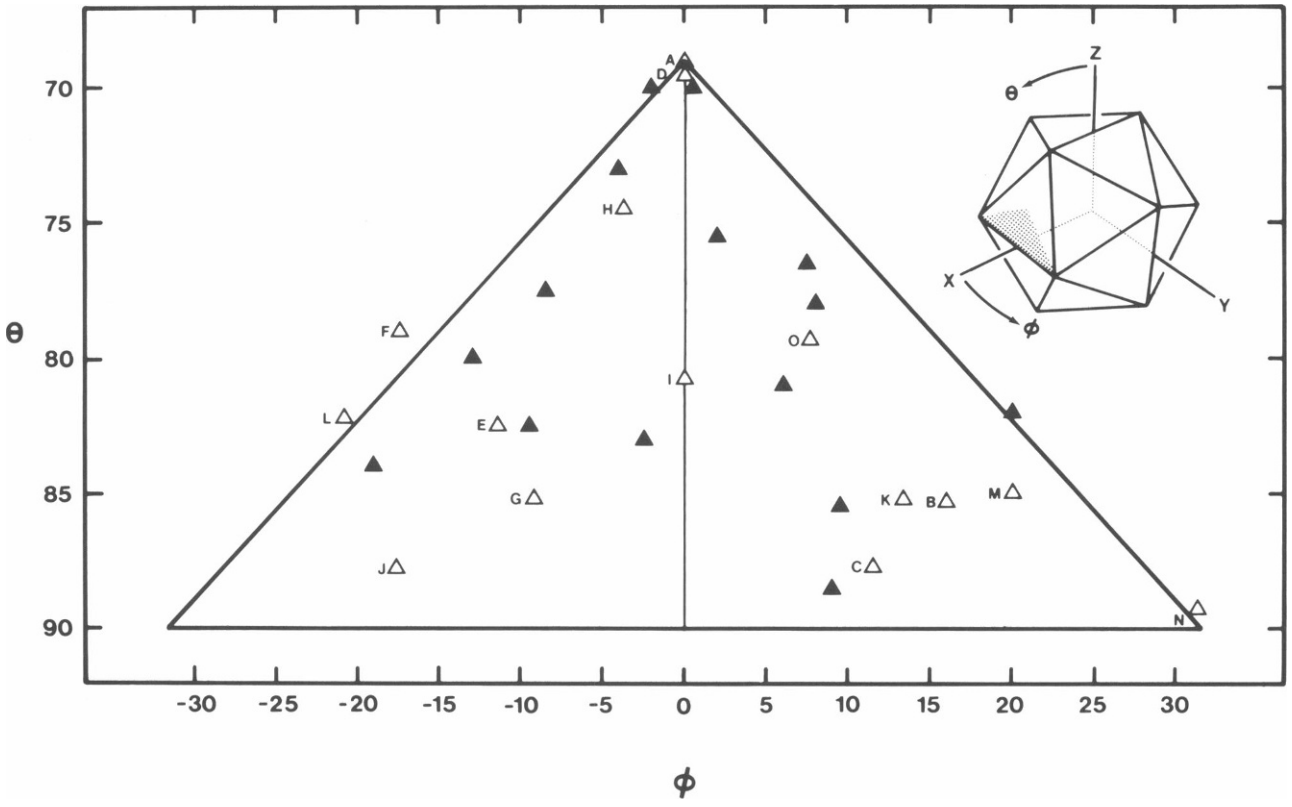

FIGURE 3 Plot of the refined view orientations (θ, ϕ) determined for the SV40 particle images used to reconstruct the three-dimensional structure displayed in Fig. 5. The labeled, open triangles correspond to the 15 particles labeled in Figs. 1 and 6. The large triangle, representing one of the 60 equivalent icosahedral asymmetric units (shaded region of inset), identifies views in the chosen coordinate frame with θ values ranging from 69 to 90° and ϕ values ranging from −32 to 32°. The top corner (θ, ϕ = 69.09, 0.0) corresponds to the view along a three-fold icosahedral axis of symmetry and the bottom two corners (θ, ϕ = 90.0, −31.72, and 90.0, 31.72) correspond to two adjacent five-fold views. The vertical line divides the asymmetric unit in half such that particles viewed along θ, ϕ are enantiomorphs of particles viewed along θ, $-\phi$. Particle G (θ, ϕ = 85, −10) and the unlabeled particle (*solid triangle* at θ, ϕ = 85, 10) are nearly mirror images of one another (data not shown). The base of the vertical line marks the two-fold view orientation (θ, ϕ = 90.0, 0.0). Particles viewed close to an equatorial direction (e.g., I on the vertical line or A, L, or N on lines marking the boundary of the asymmetric unit) display a mirror line of symmetry in the projected image (see Fig. 6). The inset drawing schematically identifies the asymmetric unit (*shaded portion*) of a strict icosahedron and the convention for specifying the view orientation (θ, ϕ), as adopted by Klug and Finch (1968). The *x*, *y*, *z* Cartesian coordinate frame is arranged to coincide with three mutually-perpendicular two-fold axes of the icosahedron.

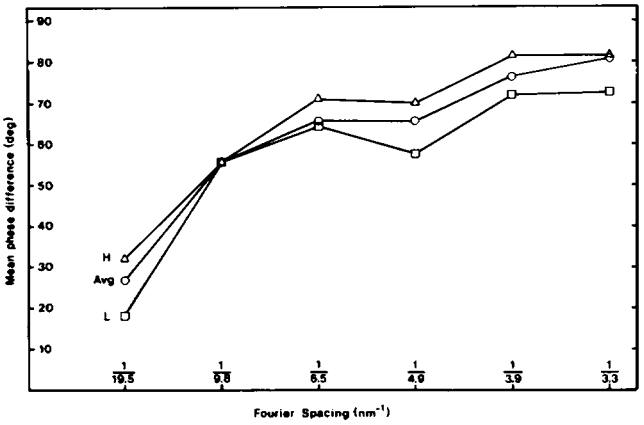

FIGURE 4 Plot showing the icosahedral correlation as a function of increasing spatial frequency for (O) the average of the 30 particles used in the reconstruction shown in Fig. 5, (△) one of the best images and (□) one of the poorest. The mean phase difference is measured on lines in the Fourier transform of the image related by the symmetry elements. A value of 90° represents random correlation along the common transform lines, whereas lower values result from good correlation with icosahedral symmetry.

cies plotted in Fig. 4. To achieve a significant reduction in noise, a relatively large number of particle images were used to compute the three-dimensional reconstructions. The thirty images selected from the micrograph (Fig. 1) showed the highest correlation with icosahedral symmetry.

Three-dimensional structure of simian virus 40

Two reconstructions of the mature simian virus 40 structure were computed from two independent sets of data, each containing fifteen particle images. Because the two reconstructions appear identical within experimental uncertainty, the entire set of 30 particles images was combined to compute the average reconstruction shown in Fig. 5. The projected density maps clearly show that both the pentavalent and hexavalent capsomeres have pentameric substructure (Fig. 5, *A*, *C*, *E*). The two types of capsomeres have nearly the same size and mass, as might be expected for pentameric oligomers composed of a single protein (VP1).

Confidence in the structure obtained by the image analysis procedures was qualitatively assessed by comparing each original particle image with the corresponding back-projected view of the reconstruction. Fig. 6 shows the results obtained for the 15 particles used in the first reconstruction. Similar results were seen for the second set of 15 particles. Close inspection of the gallery of comparisons demonstrates that most of the prominent

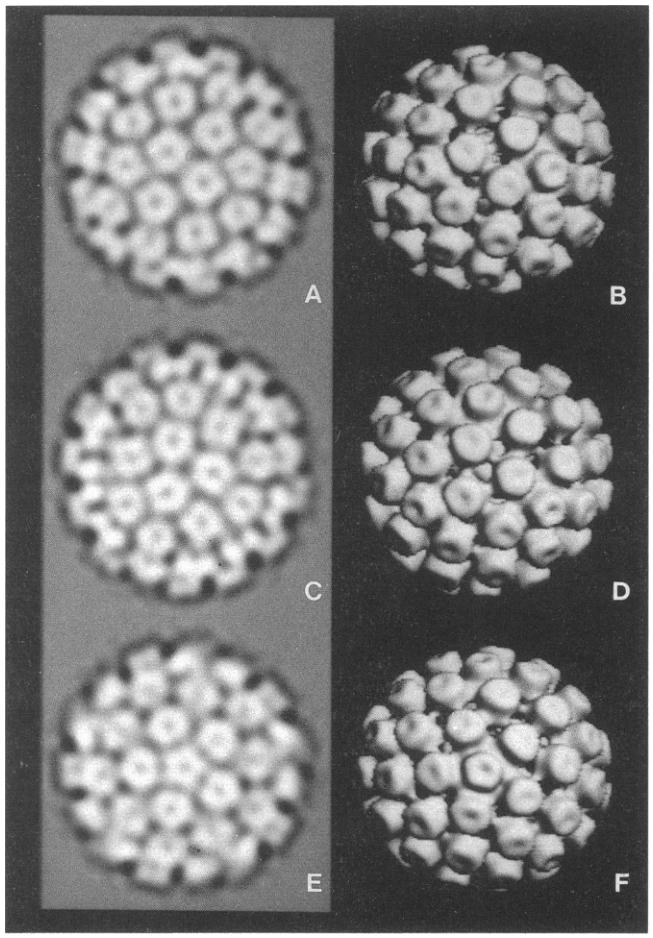

FIGURE 5 Three-dimensional electron density reconstruction computed from 30 particle images. Density maps of the top half of particles are projected down the icosahedral two- (*A*), three-, (*C*), and five-fold (*E*) axes. Solid-model, surface shaded representations of the respective views are shown in *B*, *D* and *F*.

superposition features in each noisy image are faithfully represented in the reconstruction (Fig. 6). This verifies that all particle images were included in the reconstruction with essentially correct view parameters.

Surface views of the SV40 virion reconstruction show prominent cylindrical cap regions which protrude from an underlying shell region (Fig. 5, *B*, *D*, *F*). This suggests that, in the capsid, the VP1 subunits in the capsomeres consist of two major structural domains, one protruding in a radial direction and the other extending tangentially at lower radii. The shell region of the capsid appears perforated, especially at the icosahedral three-fold axes (Figs. 5 *D* and 7). These holes may provide access for small molecules to the minichromosome inside the virion. Inspection of the electron density confined in a relatively uniform spherical region inside the inner boundary of the capsid, corresponding to the nucleohistone core, indicates

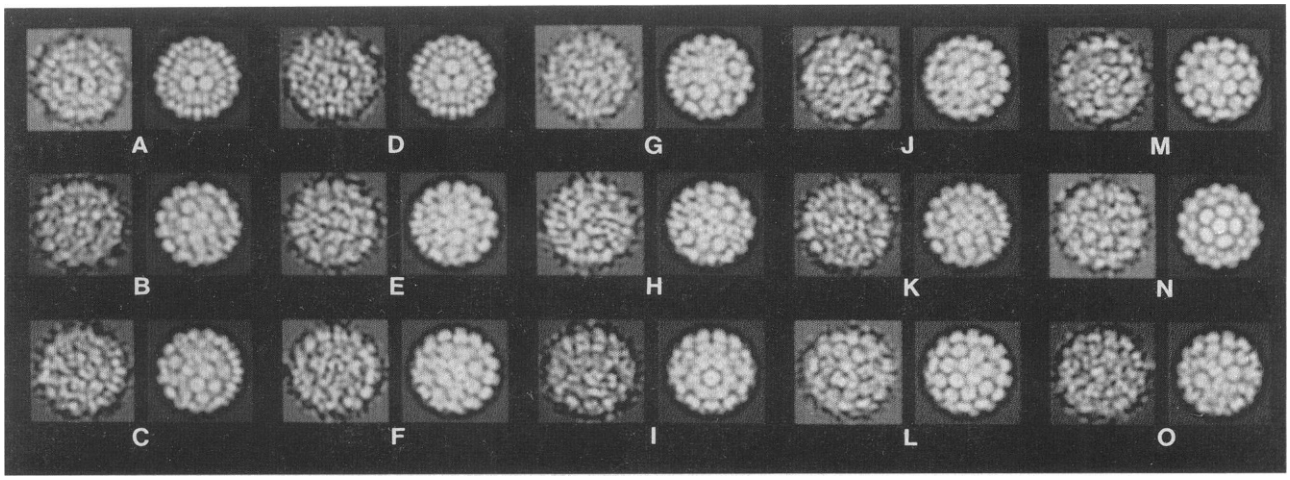

FIGURE 6 Gallery of views comparing original individual particle images (*left image of each pair*) with corresponding projected views of one of the two 15-particle three-dimensional reconstructions (*right column*). The original images have been Fourier filtered, to remove noise at spatial frequencies finer than 3.8 nm, and contrast enhanced for comparison with the reconstructed images. Close inspection of each pair reveals that the prominent features (superposition patterns) in the reconstructed images are clearly represented in the original noisy images, substantiating that the three-dimensional reconstruction is correctly determined to 3.8 nm resolution.

that the minichromosome is not organized with icosahedral symmetry matching that of the capsid (Baker et al., 1988) (Fig. 7, *E* and *G*). Weak density which extends along the axis of the pentavalent pentamers towards the virion center may correspond to a region of contact between VP1 and the nucleohistone core or to the location of the minor proteins, VP2 and VP3.

Comparative analysis of SV40 and polyoma capsid structures

Fig. 7 compares the SV40 virion reconstruction with the structure of the polyoma empty capsid solved by x-ray crystallography (Rayment et al., 1982). Despite fundamental differences in the methods used to solve the structures and the different resolution of the two electron density maps, the similarity between them is remarkable. Both papova viruses display the same, previously unexpected 72 pentamer capsid structure. The pentameric substructure of the hexavalent capsomere is clearly resolved in both structures (Fig. 7 *A–D*).

The SV40 reconstruction independently verifies the fact that the capsid of polyoma is composed of 72 pentameric capsomeres. This resolves questions previously raised about the validity of the crystallographic methods used for solving the polyoma structure (Eisenberg, 1982; Klug, 1983). Additional evidence showing that polyoma VP1 only forms pentamers has been provided by electron microscopy and image analysis of (*a*) polymorphic tube aggregates isolated from infected cells (Baker et al., 1983), and (*b*) the pentameric and capsid-like structures obtained using polyoma VP1 expressed in *E. coli* (Salunke et al., 1986).

The finding that both types of capsomeres consist of VP1 pentamers (Figs. 5 and 7) explains why the three-dimensional reconstruction of negatively-stained polyoma virions revealed hexavalent and pentavalent capsomeres of nearly the same size (Finch, 1974). Although the pentameric substructure of both types of capsomeres is clearly revealed in the 3.8 nm resolution SV40 reconstruction, capsomere substructure was not observed in the 2.5 nm resolution polyoma reconstruction. Differences in the polyoma and SV40 image reconstructions can be partly attributed to differences in the mechanisms of contrast formation between stained and unstained samples. Negative-staining mainly reveals external surface features (Haschemeyer and Myers, 1970; Horne and Wildy, 1979; Oliver, 1973), whereas, contrast in frozen-hydrated specimens is formed at internal as well as external protein-water interfaces (Chiu, 1986; Stewart and Vigers, 1986). Pentameric substructure may not have been revealed in the polyoma reconstruction (Finch, 1974) since the outer surface of the projecting domain of the capsomere is roughly cylindrical in shape (Fig. 4 *D*, *E*, *F*). Features which give rise to the five-fold modulation in the projected capsomere electron density mainly arise from portions of the capsomere which may be inaccessible to stain. Additional differences in the two reconstructions may be attributed to radiation induced movement of the negative stain (Unwin, 1974) as well as other radiation

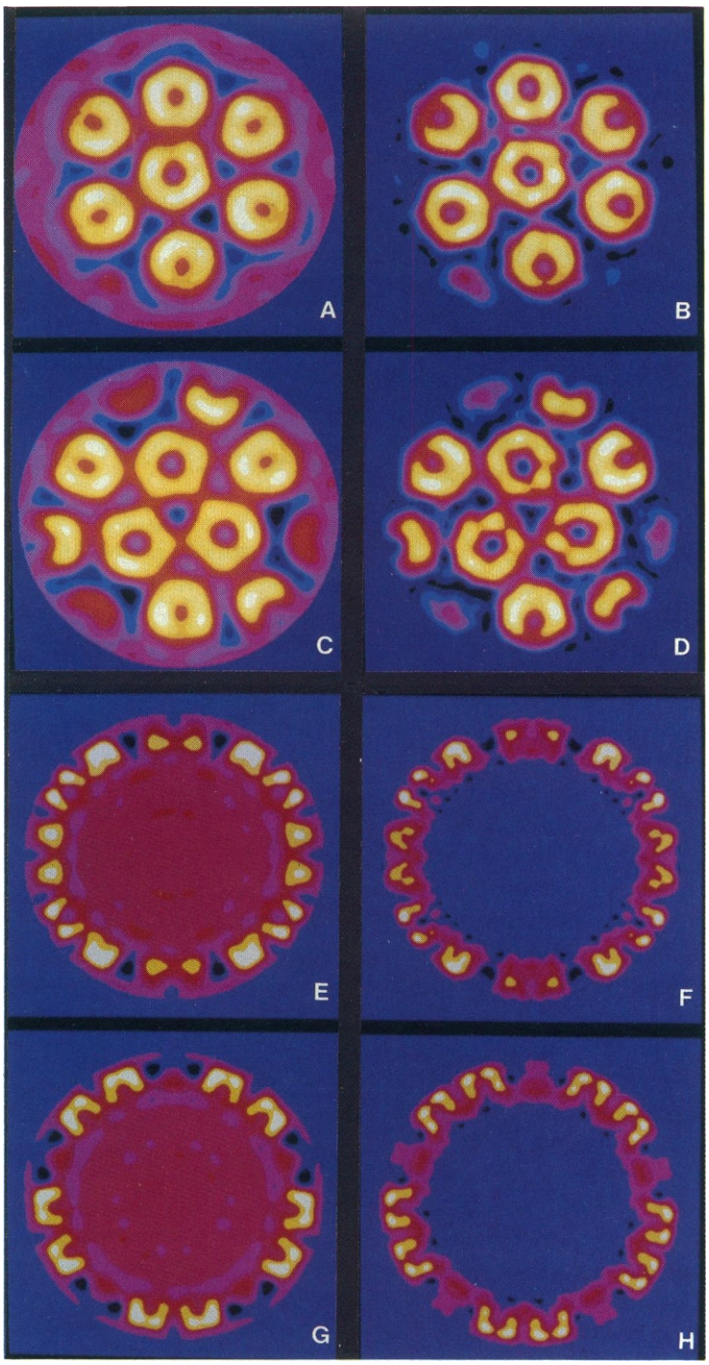

FIGURE 7 Comparison of the SV40 image reconstruction (*A*, *C*, *E*, *G*) with the electron density map of the polyoma capsid (*B*, *D*, *F*, *H*) obtained by x-ray crystallography (Rayment et al., 1982). (*A–D*) are half-particle projections viewed close to the axis of the hexavalent capsomere (*A*, *B*) and along the icosahedral three-fold axis (*C*, *D*), revealing the pentameric substructure of the capsomeres in both viruses. The structural features appear quite similar in the comparable views (*A–D*). The higher overall intensity in the SV40 views (*A*, *C*) arises from density in the virion core which is projected along with the capsid density. Contributions from the core density are not observed in projections of thinner sections through the capsid (not shown). Central sections of the structures viewed along the two-fold (*E*, *F*) and five-fold (*G*, *H*) directions show (*a*) a clear break (lower density) in the region separating the chromatin core from the inner boundary of the protein shell and (*b*) the cross-sectional profile of the capsomeres. The look-up tables at the left identify how the range of electron densities in the maps are color-coded in the images (brighter colors represent higher electron density features).

effects in the polyoma samples in which a high electron dose was required for microscopy (Finch, 1974).

Detailed, quantitative comparisons of the SV40 reconstruction and the x-ray structure of the polyoma capsid (Fig. 7) show excellent correspondence between the two structures, within the errors of measurement. The outer diameter of both virus particles is the same (Table 1). The size, shape, radial extent, and intersubunit contacts in the two types of capsomeres also closely compare. In both maps, the pentavalent pentamer is radially displaced 0.2–0.4 nm farther from the particle center than the hexavalent pentamer. Most differences in the maps can be attributed to the higher resolution of the crystallographic study (Rayment et al., 1982). Furthermore, the comparison of "full" and "empty" capsids demonstrates that the loss of minichromosomes does not noticeably alter the capsid structure.

CONCLUSIONS

The capsid structures of SV40 and polyoma are essentially indistinguishable at low resolution. Consequently, it is likely that other members of the papovavirus *B* genus (K, RKV, BK and JC) have similar capsid structures. The existence of capsid structures of opposite hand such as human wart ($T = 7d$) and rabbit papilloma ($T = 7l$), raises questions concerning the VP1 bonding specificity and the roles of minor proteins in the assembly and the structure of the virus shell. Higher resolution studies are required to identify how antigenic determinants and other phenotypic properties, which distinguish viruses of the papova family, arise from differences in the primary amino acid sequences of the virion proteins.

In addition to VP1 and the nucleohistone core, SV40 virions contain two minor proteins, VP2 and VP3. The location of these two proteins in the virion structure and their functions are still unknown. Development of more refined image analysis procedures and the application of electron microscopic labeling techniques may help locate these proteins and also provide information about the structure of the nucleohistone core. Because inside the virion the nucleohistone core may have an asymmetric organization, its structure cannot be studied by conventional crystallographic analysis. Application of single-particle image analysis procedures may provide a rational approach for probing the complete structure of the papova viruses.

We thank P. N. T. Unwin and colleagues for helpful discussions and their assistance with the cryo-microscopy of SV40, and for use of the Stanford University electron microscope facilities. We thank N. Olson for technical assistance; L. A. Amos and R. A. Crowther, and S. Fuller for icosahedral image processing programs; M. Radermacher for the surface shading algorithm; and D. L. D. Caspar, D. J. DeRosier, W. T. Murakami, G. Sosinisky, and I. Rayment for advice.

Timothy S. Baker is supported by research grants from National Institutes of Health and start-up funds from Purdue University (Department of Biological Sciences and the Showalter Fund), the Indiana Elks, and the American Cancer Society. Minou Bina is supported by research grants from National Science Foundation and American Cancer Society.

Received for publication 6 June 1988 and in final form 13 September 1988.

REFERENCES

Adrian, M., J. Dubochet, J. Lepault, and A. W. McDowall. 1984. Cryo-electron microscopy of viruses. *Nature (Lond.)* 308:32–36.

Anderer, F. A., H. D. Schlumberger, M. A. Koch, H. Frank, and H. J. Eggers. 1967. Structure of simian virus 40. II. Symmetry and components of the virus particle. *Virology.* 32:511–523.

Baker, T. S., and L. A. Amos. 1978. Structure of the tubulin dimer in zinc-induced sheets. *J. Mol. Biol.* 123:89–106.

Baker, T. S. 1981. Image processing of biological specimens: a bibliography. *Elec. Microsc. in Biol.* 1:189–290.

Baker, T. S., D. L. D. Caspar, and W. T. Murakami. 1983. Polyoma virus 'hexamer' tubes consist of paired pentamers. *Nature (Lond.).* 303:446–448.

Baker, T. S., J. Drak, and M. Bina. 1985. Cryo-electron microscopy and image analysis of SV40. *Proc. 43rd Ann. Meet. Elec. Microsc. Soc. Am.* 43:316–317.

Baker, T. S., and I. Rayment. 1987. *In* Animal Virus Structure. M. V. Nermut and A. C. Steven, editors, Elsvier Science Publishers. 335–348.

Baker, T. S., J. Drak, and M. Bina. 1988. Reconstruction of the three-dimensional structure of simian virus 40 and visualization of the chromatin core. *Proc. Natl. Acad. Sci. USA* 85:422–426.

Baumgartner, I., C. Kuhn, and E. Fanning. 1979. Identification and characterization of fast-sedimenting SV40 nucleoprotein complexes. *Virology.* 96:54–63.

Bina, M., S. Beecher, and V. Blasquez. 1982. The stability and components of mature simian virus 40. *Biochemistry.* 21:3057–3063.

Bina, M. 1986. Simian virus 40 assembly. *Comments Mol. Cell Biophys.* 4:55–62.

Blasquez, V., S. Beecher, and M. Bina. 1983. Simian virus 40 morphogenetic pathway: an analysis of assembly-defective tsB201 DNA-protein complexes. *J. Biol. Chem.* 258:8477–8484.

Caspar, D. L. D., and A. Klug. 1962. Physical principles in the construction of regular viruses. *C. S. H. Symp. Quant. Biol.* 27:1–24.

Chiu, W. 1986. Electron microscopy of frozen, hydrated biological specimens. *Annu. Rev. Biophys. Biophys. Chem.* 15:237–257.

Crowther, R. A., D. J. DeRosier, and A. Klug. 1970*a*. The reconstruction of a three-dimensional structure from projections and its application to electron microscopy. *Proc. Roy. Soc. Lond. A* 317:319–340.

Crowther, R. A., L. A. Amos, J. T. Finch, D. J. DeRosier, and A. Klug. 1970*b*. Three dimensional reconstructions of spherical viruses by Fourier synthesis from electron micrographs. *Nature (Lond.).* 226:421–425.

Crowther, R. A. 1971. Procedures for three-dimensional reconstruction of spherical viruses by Fourier synthesis from electron micrographs. *Phil. Trans. R. Soc. Lond. B.* 261:221–230.

Crowther, R. A., and L. A. Amos. 1971. Harmonic analysis of electron microscope images with rotational symmetry. *J. Mol. Biol.* 60:123–130.

DeRosier, D. J., and P. B. Moore. 1970. Reconstruction of three-dimensional images from electron micrographs of structures with helical symmetry. *J. Mol. Biol.* 52:355–369.

Eisenberg, D. 1982. A problem for the theory of biological structure. *Nature (Lond.).* 295:99–100.

Erickson, H. P., and A. Klug. 1971. Measurement and Compensation of Defocusing and Aberrations by Fourier Processing of Electron Micrographs. *Phil. Trans. R. Soc. Lond. B* 261:105–118.

Fernandez-Munoz, R., M. Coca-Prados, and M. T. Hsu. 1979. Intracellular forms of simian virus 40 nucleoproteins complexes. I. Methods of isolation and characterization in CV-1 cells. *J. Virol.* 29:612–623.

Finch, J. T., and A. Klug. 1965. The structure of viruses of the papilloma-polyoma Type. III. Structure of rabbit polyoma virus. *J. Mol. Biol.* 13:1–12.

Finch, J. T. 1974. The surface structure of polyoma. *J. Gen. Virol.* 24:359–364.

Friedmann, T., and D. David. 1972. Structural roles of polyoma virus proteins. *J. Virol.* 10:776–782.

Fuller, S. 1987. The T=4 envelope of sindbis virus is organized by interactions with a complementary T=3 capsid. *Cell.* 48:923–934.

Garber, E., M. Seidman, and A. J. Levine. 1979. The detection and characterization of multiple forms of SV40 nucleoprotein complexes. *Virology* 90:305–316.

Griffith, J. 1975. Chromatin structure: deduced from a minichromosome. *Science (Wash. DC).* 187:1202–1203.

Haschemeyer, R. H., and R. J. Myers. 1970. Negative staining. *Princ. Tech. Elec. Microsc.* 2:99–147.

Horne, R. W., and P. Wildy. 1961. Symmetry in virus architecture. *Virology.* 15:348–373.

Horne, R. W., and P. Wildy. 1979. An historical account of the development and applications of the negative staining technique to the electron microscopy of viruses. *J. Microsc.* 117:103–122.

Klug, A. 1965. Structure of viruses of the papilloma-polyoma type II. Comments on other work. *J. Mol. Biol.* 11:424–431.

Klug, A., and J. T. Finch. 1965. Structure of virus of the papilloma-polyoma type. I. Human wart virus. *J. Mol. Biol.* 11:403–423.

Klug, A., and J. T. Finch. 1968. Structure of viruses of the papilloma-polyoma Type IV. Analysis of tilting experiments in the electron microscope. *J. Mol. Biol.* 31:1–12.

Klug, A. 1983. Architectural design of spherical viruses. *Nature (Lond.).* 303:378–379.

Lepault, J., and K. Leonard. 1985. Three dimensional structure of unstained, frozen-hydrated extended tails of bacteriophage T4. *J. Mol. Biol.* 182:431–441.

Mattern, C. F. T. 1962. Polyoma and papilloma viruses: do they have 42 or 92 subunits? *Science (Wash. DC).* 137:612–613.

Mayor, H. D., and J. L. Melnick. 1962. Icosahedral models and viruses: a critical evaluation. *Science (Wash. DC).* 137:613–615.

Melnick, J. L. 1962. Papova virus group. *Science (Wash. DC).*135:1128–1130.

Milligan, R. A., A. Brisson, and P. N. T. Unwin. 1984. Molecular structure determination of crystalline specimens in frozen aqueous solutions. *Ultramicroscopy.* 13:1–10.

Oliver, R. M. 1973. Negative stain electron microscopy of protein macromolecules. *Meth. Enzymol.* 27:616–672.

Rayment, I., T. S. Baker, D. L. D. Caspar, and W. T. Murakami. 1982. Polyoma virus capsid structure at 22.5 Å resolution. *Nature (Lond.).* 295:110–115.

Salunke, D. M., D. L. D. Caspar, and R. L. Garcea. 1986. Self-assembly of purified polyomavirus capsid protein VP1. *Cell.* 46:895–904.

Sharp, D. G., A. R. Taylor, D. Beard, and J. W. Beard. 1942. Study of the papilloma virus protein with the electron microscope. *Proc. Soc. Exp. Biol. and Med.* 50:205–207.

Stewart, M., and G. Vigers. 1986. Electron microscopy of frozen-hydrated biological material. *Nature (Lond.).* 319:631–636.

Tooze, J. 1981. *DNA Tumor Viruses, Molecular Biology of Tumor Viruses,* Part 2, Cold Spring Harbor Laboratory, Cold Spring Harbor, NY.

Unwin, P. N. T. 1974. Electron microscopy of the stacked disk aggregate of tobacco mosaic virus protein. II. The influence of electron irradiation on the stain distribution. *J. Mol. Biol.* 87:657–670.

Wildy, P., M. G. P. Stokes., I. A. Macpherson, and R. W. Horne. 1960. The fine structure of polyoma virus. *Virology.* 11:444–457.

Yuen, L. K. C., and R. A. Consigli. 1985. Identification and protein analysis of polyomavirus assembly intermediates from infected primary mouse embryo cells. *Virology.* 144:127–138.

Williams, R. C., and H. W. Fisher. 1970. Electron microscopy of tobacco mosaic virus under conditions of minimal beam exposure. *J. Mol. Biol.* 52:121–123.